KURENAI
Kyoto University Research Information Repository

KYOTO UNIVERSITY

Title	Analysis of Particle-Size Distributions by a Dynamic Light Scattering Apparatus with a Time Interval Digitizer (Special Issue on Polymer Chemistry, XVI)
Author(s)	Tsunashima, Yoshisuke; Nemoto, Norio; Makita, Yutaka; Kurata, Michio
Citation	Bulletin of the Institute for Chemical Research, Kyoto University (1981), 59(4): 293-309
Issue Date	1981-11-30
URL	http://hdl.handle.net/2433/76950
Right	
Type	Departmental Bulletin Paper
Textversion	publisher

Kyoto University

Analysis of Particle-Size Distributions by a Dynamic Light Scattering Apparatus with a Time Interval Digitizer

Yoshisuke Tsunashima, Norio Nemoto, Yutaka Makita, and Michio Kurata*

The Histogram method presented by Chu *et al.* for analyzing the correlation function profile measured by means of homodyne photon correlation spectroscopy is reexamined and its reliability is established for a wide variety of autocorrelation functions consisting of bimodal modes. The autocorrelation functions analyzed are simulated test functions which are constructed for a hypothetical system with bimodal particle-size distributions, and observed functions which are obtained by a computer-controlled software correlator with 512 channels for aqueous suspensions of binary mixtures of polystyrene-latex particles of different known radii.

I. INTRODUCTION

The dynamic light scattering method is extensively used in the study of polymer chain dynamics as a powerful tool to analyze diffusive motions in solutions.[1~3]   However, the analysis is often obstructed by the existence of polydispersity in polymer samples or by the appearance of intramolecular motions.   These effects distort the shape of the autocorrelation function $A(\tau)$ measured by photon correlation spectroscopy from a single exponential form, and more or less complicate interpretation of the measured function.

Recently, Chu and his collaborators including one of the present authors have proposed a histogram method for analyzing the correlation function profile of non-exponential decay.[4] In this method, the normalized distribution function of the decay rate, $G(\Gamma)$, is approximated by an equally segmented histogram in Γ space and the histogram is determined so as to minimize a measure of fitness of the computed $A(\tau)$ to the experimental one with respect to the histogram parameters, cf. seq.   With $A(\tau)$ composed of 96 delay channel numbers, Chu *et al.* have studied the reliability of the histogram method by simulation and predicted that if the disturbance from intramolecular motions is absent, the method should be fairly applicable to the analysis of the polydispersity in macromolecular samples with either unimodal or bimodal distribution of molecular weight.   They have successfuly tested this prediction by using aqueous suspensions of a polystyrene(PS)-latex[4] and two low-molecular-weight polystyrene $(M_w=1.03\times10^4$ and $1.79\times10^5)$ in cyclohexane.[5]   All these solutes, however, have unimodal distributions of particle or molecular dimensions.

---

* 綱島良祐, 根本紀夫, 槇田　穰, 倉田道夫 : Laboratory of Polymer Physical Chemistry, Institute for
Chemical Research, Kyoto University, Uji, Kyoto 611.

Thus, the reliability of the histogram method has not fully been established yet for systems with bimodal particle-size distributions.

We have recently constructed a computer-controlled software correlator with a channel number as large as 512.[6] The increase in the channel number up to 512 was naturally effective in locating the base-line level on the diagram for observed photon correlations, and allowed us to shape an accurate autocorrelation function $A(\tau)$ even for very weak scattered intensity at scattering angles ranging from 10° to 150°. Thus, we are in a position to try an accurate analysis of $A(\tau)$, especially consisting of double or multiple mode distributions in the decay rate. For example, we are interested in separate determination of diffusive and intramolecular modes from $A(\tau)$ of a high-molecular-weight polymer sample, or in separation of two translational diffusive modes of a mixture of two kinds of particles or molecules with distinctly different dimensions. For the purpose, we employ the histogram method mentioned above.

In this article, we first review the histogram method of analysis and then apply it to a series of simulated autocorrelation functions $A(\tau)$ which are constructed for various types of bimodal particle-size distributions with taking a plausible disturbance from noise into account. Comparison of the particle-size distribution recovered from $A(\tau)$ with the one originally set in the simulation allows us to estimate the reliability of the histogram method of analysis employed. The histogram method is also applied to mixtures of two kinds of aqueous PS-latices, each bearing a unimodal particle-size distributions around a mutually different mean value. It will be shown that the particle-size distribution of each component latex is actually derivable by using the histogram method from $A(\tau)$ obtained for the mixtures.

II. HISTOGRAM METHOD

1. Unimodal System

When an optical field obeys Gaussian statistics, the normalized photocurrent autocorrelation function measured by the homodyne method, $A(\tau)$, is related to the normalized first-order correlation function of the scattered electric field, $g^{(1)}(\tau)$ as

$$A(\tau)=1+\beta|g^{(1)}(\tau)|^2 \tag{1}$$

where τ is the delay time and β is the amplitude dependent on experimental condition of coherence. β is usually assumed to be an unknown parameter in the data fitting procedure.

For a monodisperse polymer solution, $g^{(1)}(\tau)$ can be written as·

$$|g^{(1)}(\tau)|=\exp(-\varGamma\tau) \tag{2}$$

if the contribution of intramolecular motions is negligible. The decay rate $\varGamma$ is related to the diffusion coefficient D as

$$\varGamma=Dq^2 \tag{3}$$

with

$$q=(4\pi n/\lambda_0)\sin(\theta/2) \tag{4}$$

where n is the refractive index of solvent, λ_0 the wavelength of the incident light in vacuum,

and θ the scattering angle. For a system with a continuous distribution of Γ, the function $g^{(1)}(\tau)$ can be expressed as

$$|g^{(1)}(\tau)| = \int_0^\infty G(\Gamma)\exp(-\Gamma\tau)d\Gamma \qquad (5)$$

where $G(\Gamma)\,d\Gamma$ represents the fraction of the total integrated intensity of scattered light from the molecules with decay rates between Γ and $\Gamma+d\Gamma$. In the histogram method, Eq. (5) is approximated by a histogram of equally segmented steps $\Delta\Gamma$ in Γ-space:

$$|g^{(1)}(\tau)| = \sum_{j=1}^{M} H_j(\Gamma_j) \int_{\Gamma_j-\Delta\Gamma/2}^{\Gamma_j+\Delta\Gamma/2} \exp(-\Gamma i\Delta\tau)d\Gamma \qquad (6)$$

with the normalization condition,

$$\sum_{j=1}^{M} H_j(\Gamma_j)\Delta\Gamma = 1 \qquad (7)$$

Here $H_j(\Gamma_j)$ is the height of the j-th histogram step of the width $\Delta\Gamma$ around Γ_j and M is the number of steps. Hence,

$$\Delta\Gamma = (\Gamma_{\max} - \Gamma_{\min})/M \qquad (8)$$

$\Delta\tau$ is the clock pulse interval for our time interval correlator, and i is the channel number (≤ 511) with $\tau = i\Delta\tau$.

Substituting Eq. (6) into Eq. (1), we obtain the fitting error Δ_i for the i-th channel as

$$\Delta_i = [A(i\Delta\tau)-1] - \beta \Big[\sum_{j=1}^{M} \{-H_j(\Gamma_j)/i\Delta\tau\} \times$$

$$\Big\{ \exp\Big[-\Big(\Gamma_j+\frac{1}{2}\Delta\Gamma\Big)i\Delta\tau\Big] - \exp\Big[-\Big(\Gamma_j-\frac{1}{2}\Delta\Gamma\Big)i\Delta\tau\Big]\Big\}\Big]^2 \qquad (9)$$

Then, values of $H_j(\Gamma_j)$ can be obtained by using the non-linear least-square fitting procedure where the reduced sum of $\Delta_i{}^2$ is minimized with respect to a set of $H_j(\Gamma_j)$:

$$\frac{\partial}{\partial H_j(\Gamma_j)} \sum_{i=1}^{511} (\Delta_i{}^2/\sigma_i{}^2) = 0 \quad (j=1, 2, ..., M) \qquad (10)$$

where $\sigma_i{}^2$ is the statistical fluctuation of data point. The algorithm of Marquardt[7] was practically in use because of its rapid convergence and good fitness.

In the fitting procedure, the initial values of $H_j(\Gamma_j)$ and of Γ range ($\Gamma_{\min}$ and $\Gamma_{\max}$) are to be refined after each computation. The refinement of the former is immaterial, but some care may be required for the latter. We searched the Γ range by setting $H_j(\Gamma_j)$ equal to zero when its contribution is less than 0.5% of the maximam value of H_j. Computations were carried out by a FACOM M-160AD computer in our institute.

2. Bimodel System

When the resultant histogram shows a bimodal-like distribution, the measured auto-correlation function $A(i\Delta\tau)$ may be re-analyzed by a splitted bimodal distribution with $g^{(1)}(\tau)$ in the form

$$|g^{(1)}(\tau)| = \sum_{l=1}^{2} \sum_{j_l=1}^{M_l} H_{jl}(\Gamma_{jl}) \int_{\Gamma_{jl}-\Delta\Gamma_l/2}^{\Gamma_{jl}+\Delta\Gamma_l/2} \exp(-\Gamma i\Delta\tau)d\Gamma \qquad (11)$$

with the normalization condition,

Y. Tsunashima, N. Nemoto, Y. Makita, and M. Kurata

$$\sum_{l=1}^{2} \sum_{j_l=1}^{M_l} H_{jl}(\Gamma_{jl})\Delta\Gamma_l = 1 \tag{12}$$

Here $H_{jl}(\Gamma_{jl})$, $\Delta\Gamma_l$, and M_l bear the same meanings as before within each mode denoted by l. The relative intensity of each mode is therefore obtained as the amplitude at $\tau=0$ in Eq. (11),

$$a_l = \sum_{j_l=1}^{M_l} H_{jl}(\Gamma_{jl})\Delta\Gamma_l, \quad l=1, 2. \tag{13}$$

3. Mean Decay Rate and Cumulants

The relationship between the cumulant and the moment expressions for $g^{(1)}(\tau)$ gives us[1,2,8]

$$\ln|g^{(1)}(\tau)| = \sum_{n=1}^{\infty} K_n(\Gamma)\{(-\tau)^n/n!\}$$

$$= -\bar{\Gamma}\tau + \frac{1}{2!}\mu_2\tau^2 - \frac{1}{3!}\mu_3\tau^3 + \frac{1}{4!}(\mu_4 - 3\mu_2{}^2)\tau^4 - \cdots \tag{14}$$

where K_n is the n-th cumulant, and μ_n is the n-th moment about the mean of $G(\Gamma)$:

$$\mu_n = \int_0^{\infty} (\Gamma - \bar{\Gamma})^n G(\Gamma)d\Gamma \tag{15}$$

Thus, the profile of Γ distribution will be expressed by the following values,

$$K_1 = \mu_1 = \bar{\Gamma} = \int_0^{\infty} \Gamma G(\Gamma)d\Gamma = \langle D \rangle_z q^2,$$

$$K_2 = \mu_2, \quad K_3 = \mu_3, \quad K_4 = \mu_4 - 3\mu_2{}^2, \cdots \tag{16}$$

where $\bar{\Gamma}$ is the mean decay rate, $\langle D \rangle_z$ is the z-average diffusion coefficient. $\mu_2/\bar{\Gamma}^2$, $\sqrt{\mu_2}$, $\mu_3/\mu_2{}^{3/2}$, and $\mu_4/\mu_2{}^2$ represent the z-average normalized variance, the standard deviation, the skewness (asymmetricity), and the curtosis (peakness) of the distribution, respectively. Terminating Eq. (14) at K_n term and substituting it into Eq. (1), we can obtain the optimum values for the first to n-th cumulants and moments by using the minimization algorithm of Marquardt mentioned above. The results are then called the n-th-order fit of the cumulants method.[8] It should be noted that the cumulants method can never predict the presence of bimodal nor multimodal distribution, but analyze the distribution as a unimodal one.

III. SIMULATED DATA ANALYSIS

1. Simulated Data Generation

The normalized and substantial autocorrelation function $\beta|g^{(1)}(\tau)|^2$ with bimodal distribution was generated by using a Pearson type I distribution function for $G(\Gamma)$. This function is expressed as $G(\Gamma) = C(\Gamma/h_1 - 1)^{m_1}(1 - \Gamma/h_2)^{m_2}$ with Γ ranging from h_1 to h_2. Hence,

$$\beta|g^{(1)}(i\Delta\tau)|^2 = F^*\left\{\int_{h_1}^{h_2} G_1(\Gamma)\exp(-\Gamma i\Delta\tau)d\Gamma + \right.$$

$$\left. \int_{h_3}^{h_4} G_2(\Gamma)\exp(-\Gamma i\Delta\tau)d\Gamma\right\}^2 \tag{17}$$

with

$$G(\Gamma)=G_1(\Gamma)+G_2(\Gamma)$$
$$=a_1C_1(\Gamma/h_1-1)^{m_1}(1-\Gamma/h_2)^{m_2}+a_2C_2(\Gamma/h_3-1)^{m_3}(1-\Gamma/h_4)^{m_4} \qquad (18)$$

Here a_1 and a_2 represent relative intensities of each mode, and $a_2=0$ for unimodal distribution. C_1 and C_2 are the normalization constants for $G_1(\Gamma)$ and $G_2(\Gamma)$, respectively; e.g.,

$$C_1^{-1}=\int_{h_1}^{h_2}(\Gamma/h_1-1)^{m_1}(1-\Gamma/h_2)^{m_2}d\Gamma \qquad (19)$$

$F*$ is the amplitude and its value is adjusted to be 0.75 which is a typical value obtained under our experimental condition.[6] We used an argon ion laser equipped with an etalon as light source. The integrals in Eqs. (17) and (19) were computed by using a Gauss-Legendre integral program in FACOM 230-60 Scientific Subroutine Library.

Chu et al.[4] have used in their simulation a narrow and a broad unimodal distributions of which $\mu_2/\bar{\Gamma}^2$ were 0.05 and 0.143, respectively, and bimodal distributions of which total $\mu_2/\bar{\Gamma}^2$ ranging from 0.08 to 0.97. One of the constituent mode of these bimodal distributions had a variance $\mu_{2i}/\bar{\Gamma}_i^2$ ranging from 0.259 to 2.405, and the other a rather small variance ranging from 0.00279 to 0.0108. Thus, we here test two extremely narrow unimodal distributions with variances 6.75×10^{-3} and 1.44×10^{-3}, and two bimodal distributions composed of these unimodal distributions, of which the mixing fractions of the slower decay mode a_1 are 0.30 and 0.80, respectively. The total variance of the bimodal distributions thus composed are 0.077 and 0.12 as shown in Table II.1 and II.2, respectively.

We simulated two kinds of autocorrelation functions for each distribution mentioned above, one denoted by $A'(i\Delta\tau)$ is straightforwardly evaluated by Eq. (17), and the other denoted by $A(i\Delta\tau)$ is constructed by introducing a random error factor into $A'(i\Delta\tau)$. Actually, a random number generating in the range bounded by $\pm|0.03\times A'(\Delta\tau)|$ is added to $A'(i\Delta\tau)$ at each channel. The simulated correlation function $A(i\Delta\tau)$ thus constructed shows a slightly larger scatter of data points as compared with real experimental functions. Values of parameters, h, m, a, and C, used in the simulation are listed in Table I and II.

Table I. Characterization of the simulated unimodal distribution
$$G(\Gamma)=C(\Gamma/h_1-1)^{m_1}(1-\Gamma/h_2)^{m_2}$$
$$h_1=656.5,\ h_2=970,\ m_1=1.218,\ m_2=1.344,\ C=0.3406$$

| | Calc. | Histogram Method (M=19) | | Cumulants Method | | | | | | | |
| | | no error | ±3% error | no error | | | | ±3% error | | | |
				second fit		third fit		second fit		third fit	
$\bar{\Gamma}\tau_{max}$	1.65	1.65	1.65	0.81	1.65	0.81	1.65	0.81	1.65	0.80	1.64
$\bar{\Gamma}/\text{sec}^{-1}$	808.9	808.9	808.9	809.0	809.0	809.0	809.0	807.1	808.9	798.3	804.4
$\mu_2/10^3\ \text{sec}^{-2}$	4.41	4.40	4.65	4.51	4.39	4.96	4.56	−0.151	4.04	−54.6	−13.7
$\mu_2/\bar{\Gamma}^2\times10^3$	6.75	6.73	7.10	6.90	6.70	7.58	6.97	−0.232	6.17	−85.7	−21.2
$\mu_3/10^4\ \text{sec}^{-3}$	1.17	1.10	0.958	—	—	103	23.9	—	—	−12600	−2430
$\mu_4/10^7\ \text{sec}^{-4}$	4.30	4.30	4.80	—	—	—	—	—	—	—	—
$K_4/10^7\ \text{sec}^{-4}$	−1.54	−1.51	−1.67								

Y. TSUNASHIMA, N. NEMOTO, Y. MAKITA, and M. KURATA

(298)

Table II. Characterization of the simulated bimodal distributions.

$$G(\Gamma)=a_1 C_1(\Gamma/h_1-1)^{m_1}(1-\Gamma/h_2)^{m_2}+(1-a_1)C_2(\Gamma/h_3-1)^{m_3}(1-\Gamma/h_4)^{m_4}.$$

Slow decay mode : $h_1=656.5$, $h_2=970$, $m_1=1.218$, $m_2=1.344$, $C_1=0.3406$.

Fast decay mode : $h_3=1500$, $h_4=1825$, $m_3=1.372$, $m_4=2.312$, $C_2=28.88$.

1. $a_1=0.300$

   1.1. Histogram Method ($M_1+M_2=9+10$)

	Total Values[a]			Slow Decay Mode			Fast Decay Mode		
	calc.	no error	±3% error	calc.	no error	±3% error	calc.	no error	±3% error
$\bar{\Gamma}/sec^{-1}$	1388	1388	1386	809	811	828	1636	1636	1639
$\mu_2/10^5\ sec^{-2}$	1.48	1.48	1.46	4.41 E−2[b]	5.41 E−2	5.31 E−2	3.84 E−2	4.26 E−2	4.49 E−2
$\mu_2/\bar{\Gamma}^2\times10^2$	7.66	7.66	7.59	0.675	0.823	0.773	0.144	0.159	0.167
$\mu_3/10^7\ sec^{-3}$	−4.77	−4.76	−4.33	1.17 E−3	6.65 E−3	2.97 E−3	5.38 E−3	1.65 E−3	2.69 E−3
$\mu_4/10^{10}\ sec^{-4}$	4.00	4.02	3.73	4.30 E−3	6.56 E−3	5.90 E−3	3.51 E−3	4.03 E−3	4.54 E−3
$\bar{\Gamma}\tau_{max}$	—	1.77	1.77	—	1.04	1.06	—	2.09	2.09
a_1	0.300	0.301	0.312						

   1.2. Cumulants Method[a]

	calc.	no error						±3% error					
		second fit		third fit		fourth fit		second fit		third fit		fourth fit	
$\bar{\Gamma}\tau_{max}$	—	0.69	1.77	0.69	1.77	0.69	1.77	0.69	1.77	0.69	1.77	0.67	1.77
$\bar{\Gamma}/sec^{-1}$	1388	1388	1390	1388	1388	1388	1388	1385	1388	1380	1388	1342	1386
$\mu_2/10^5\ sec^{-2}$	1.48	1.57	1.65	1.48	1.52	1.47	1.47	1.43	1.61	0.882	1.63	−7.08	1.32
$\mu_2/\bar{\Gamma}^2\times10^2$	7.66	8.16	8.53	7.70	7.88	7.66	7.63	7.45	8.36	4.63	8.44	−39.3	6.90
$\mu_3/10^7\ sec^{-3}$	−4.77	—	—	−4.06	−2.81	−4.88	−5.26	—	—	−24.6	0.355	−855	−14.8
$\mu_4/10^{10}\ sec^{-4}$	4.00	—	—	—	—	−3.60	−4.84	—	—	—	—	−3610	−29.8

2. $a_1 = 0.800$

2.1. Histogram Method ($M_1 + M_2 = 9 + 10$)

	Total Values[a]			Slow Decay Mode			Fast Decay Mode		
	calc.	no error	±3% error	calc.	no error	±3% error	calc.	no error	±3% error
$\bar\Gamma/\mathrm{sec}^{-1}$	974	974	973	809	813	812	1636	1629	1622
$\mu_2/10^5\,\mathrm{sec}^{-2}$	1.14	1.14	1.11	4.41E-2[b]	5.64E-2	5.34E-2	3.84E-2	4.35E-2	3.12E-2
$\mu_2/\bar\Gamma^2 \times 10^1$	1.20	1.20	1.17	6.75E-2	8.54E-2	7.86E-2	1.44E-2	1.65E-2	1.12E-2
$\mu_3/10^7\,\mathrm{sec}^{-3}$	5.40	5.00	4.94	1.17E-3	5.09E-3	5.44E-3	5.38E-3	4.10E-3	1.82E-2
$\mu_4/10^{10}\,\mathrm{sec}^{-4}$	4.15	3.82	3.75	4.30E-3	6.98E-3	7.27E-3	3.51E-3	4.42E-3	1.75E-3
$\bar\Gamma\tau_{max}$	—	1.99	1.99	—	1.66	1.66	—	3.36	3.36
a_1	0.800	0.806	0.809						

2.2. Cumulants Method[a]

	calc.	no error						±3% error					
		second fit		third fit		fourth fit		second fit		third fit		fourth fit	
$\bar\Gamma\tau_{max}$	—	0.97	1.98	0.97	1.99	0.97	1.99	0.97	1.97	0.97	1.99	0.96	1.99
$\bar\Gamma/\mathrm{sec}^{-1}$	974	971	966	974	974	974	974	969	965	970	974	959	972
$\mu_2/10^5\,\mathrm{sec}^{-2}$	1.14	0.917	0.791	1.13	1.10	1.14	1.14	0.879	0.777	0.925	1.15	−0.271	1.00
$\mu_2/\bar\Gamma^2 \times 10^1$	1.20	0.973	0.847	1.19	1.16	1.20	1.20	0.936	0.834	0.983	1.21	−0.294	1.06
$\mu_3/10^7\,\mathrm{sec}^{-3}$	5.40	—	—	4.98	4.40	5.60	5.78	—	—	1.08	5.35	−64.4	0.605
$\mu_4/10^{10}\,\mathrm{sec}^{-4}$	4.15	—	—	—	—	1.39	1.75	—	—	—	—	−148	−6.03

a. Total or resultant values obtained when the resulted bimodal distribution is regarded as a unimodal one.

b. For example, 1.0 E-2 = 1.0×10⁻².

Y. TSUNASHIMA, N. NEMOTO, Y. MAKITA, and M. KURATA

2. Analysis of Simulated Correlation Functions

Results of analysis of the simulated correlation function $A(i\Delta\tau)$ for the unimodal distributions are summarized in Table I. As expected, the histogram analysis of A'-functions gives all the moments except μ_3 correctly to within a 1% deviation from the input values. The analysis of A-functions to which a 3% randomization has been applied gives $\bar{\Gamma}$ correctly, μ_2 and $\mu_2/\bar{\Gamma}^2$ within a 5% deviation, and μ_3, μ_4, and K_4 within a 10% deviation from each input value, respectively. The slightly poor reproducibility of μ_3 found in the both cases indicates that the skewness of distribution, especially of narrow distribution as the present ones, is most strongly affected by the segmentation of variables as compared with other characteristics of distribution.

In the cumulant analysis, we used two different delay time ranges; one is the entire range of $i\Delta\tau$ extending from $i=1$ to 512 as is the case of the present histogram analysis, and the other is a partial space extending $i=1$ to 250. We indicate in Table I the delay time range by $\bar{\Gamma}\tau_{max}$, where τ_{max} is the maximum delay time. The cumulant method gives poorer results as compared with the histogram method; for example, the former analysis of the A-function gives $\bar{\Gamma}$ correctly but μ_2 with a 10% deviation from the input value in the second-order fit with $\bar{\Gamma}\tau_{max}=1.65$. These results indicate that the distribution used here is too narrow to be analyzed by the cumulants method.

Figure 1 shows $A(i\Delta\tau)$, which is abbreviated as $A(i)$ there, as a function of the channel number i of clock pulse interval. The percent error of fitting Δ_i given by Eq. (9) is also plotted against i. In the insert to the figure, the histogram $H_i(\Gamma_i)$ and the input Pearsonian curve are shown as functions of the decay rate Γ, where agreement between two functions
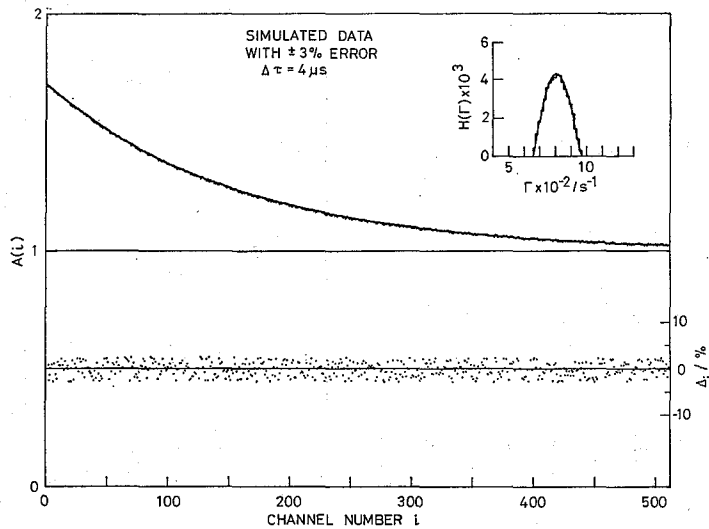

Fig. 1. The autocorrelation function $A(i)$ and the fitting error Δ_i (in %) plotted against channel number i of clock pulse interval for the simulated unimodal distribution with a 3% randomization. $A(i)$ is the abbreviation of $A(i\Delta\tau)$. Insert: The histogram $H(\Gamma)$ and the Pearsonian distribution function for the decay rate Γ. Parameter values used: $\Delta\tau=4\ \mu sec$, $\bar{\Gamma}\tau_{max}$ $=1.65$. The dots denote data points, and the solid curve $A(i)$ shows the fitting curve obtained by the histogram $H(\Gamma)$.

is excellent. Hence, using the histogram method, we can extract reliable information on $G(\Gamma)$ from $A(\tau)$ even when an extremely narrow distribution as the present one is given. It is also concluded that our choice of $\bar{\Gamma}\tau_{\max} \doteqdot 2$ is a reasonable one for precise analysis of the correlation function. Actually, $A(\tau)$ attains quite closely its base line when $\bar{\Gamma}\tau_{\max} \doteqdot 2$.

Results of the histogram analysis for two bimodal distributions defined earlier are summarized in Table II.1 and 2, the former for $a_1=0.30$ and the latter for $a_1=0.80$. In both cases, the total variance $\mu_2/\bar{\Gamma}^2$ which is a characteristic parameter in unimodal description of the bimodal distributions becomes 10 to 80 times larger than those of the constituent unimodal distributions. The total $\bar{\Gamma}$ is in agreement with the input value within 0.1% deviation, μ_2 and $\mu_2/\bar{\Gamma}^2$ within 3%, and μ_3 and μ_4 within 10%, respectively. These deviations are of comparable order with those obtained for the unimodal distributions. Furthermore, we obtained the following results for the characteristic parameters of each constituent distributions: (1) $\bar{\Gamma}$ was in agreement with the input value within 1%, (2) μ_2 and $\mu_2/\bar{\Gamma}^2$ within 25%, (3) μ_3 and μ_4 was obtained in the same order of magnitude as those of input, and (4) the relative intensity a_l of the weak mode, i.e. a_1 in Table II.1 and a_2 in Table II.2, was estimated to an accuracy of 5%. These results, especially (1) and (4), may be counted as a strong support for the reliability of the histogram method in application to the separate estimate of constituent dynamic modes from a multiple-mode correlation function. Again it is to be emphasized that we used the condition $\bar{\Gamma}\tau_{\max} \doteqdot 2$.

As shown in Table II.1 and 2, the cumulants method of third- and fourth-order fits, if used with $\bar{\Gamma}\tau_{\max} \doteqdot 2$, also gives good values of $\bar{\Gamma}$ and μ_2. However, the reliability in the estimates of higher moments rapidly decreases, and the method gives practically no information about the characteristics of each constituent distribution.

Figures 2 and 3 show plot of $A(i)$ against i, and the histograms $H_i(\Gamma_i)$ obtained from $A(i)$. Agreement of the latter with the input $G(\Gamma)$ is again satisfactory.
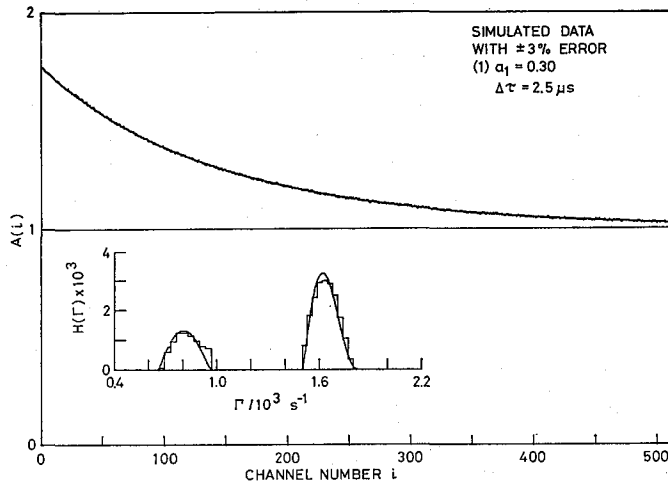

Fig. 2. Plots of $A(i)$ against i, and plots of $H(\Gamma)$ against Γ for the simulated bimodal distribution with a 3% randomization. The relative intensity of the small decay mode $a_1=0.30$. Parameter values used: $\Delta\tau=2.5\,\mu\text{sec}$, $\bar{\Gamma}\tau_{\max}=1.77$. The dots and curves bear the same meanings as in Fig. 1.
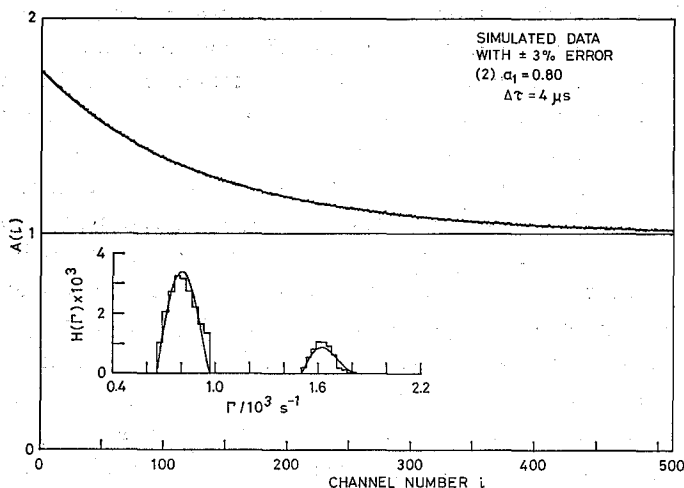
Fig. 3. Plots of $A(i)$ against i, and plots of $H(\Gamma)$ against Γ for the simulated bimodal distribution with a 3% randomization. $a_1=0.80$, $\Delta\tau=4\,\mu$sec, and $\overline{\Gamma}\tau_{max}=1.99$. The dots and curves bear the same meanings as in Fig. 1.

In conclusion, if the data-point dispersion of $A(\tau)$ is less than 3% and the range of delay time extends to $\overline{\Gamma}\tau_{max}\doteqdot 2$, we can expect the histogram method to give the characteristic parameters of bimodal distributions with the following reliances: (1) 99% on $\overline{\Gamma}$, 95% on μ_2, and 90% on μ_3 ane μ_4 for the total or overall distributions, and (2) 99% on $\overline{\Gamma}$, 75% on μ_2, an order of magnitude of μ_3 and μ_4 for each constituent distributions, and 95% on the fraction of constituent modes.

IV. MEASUREMENTS ON BINARY MIXTURES OF AQUEOUS POLYSTYRENE-LATICES

1. Particle-Size Distribution Function

Consider a polydisperse sample of spherical particles with a continuous distribution of sizes and denote by $f^*(r)dr$ the number fraction of a class of particles whose radii are in the range between r and $r+dr$. We call $f^*(r)$ the particle-size distribution. Since the molecular weight of a particle is proportional to r^3, the (number) distribution function of M is given as

$$f^*(M)=kr^2f^*(r) \tag{20}$$

where k is a constant.

According to the theory of light scattering,[9] the reduced scattered light intensity from a solution of these particles is given as

$$R(\theta)=K\nu\int_0^\infty f^*(M)M^2P(M,\theta)dM \tag{21}$$

if the molar concentration ν is sufficiently small so as to make higher order terms of ν negligible.[10] Here, θ is the scattering angle, $P(M,\theta)$ is the particle scattering factor for a particle with molecular weight M and K is a constant including the square of specific

refractive index increment. Eq. (21) can be expressed, in terms of r, as

$$R(\theta) = K'\nu \int_0^\infty f^*(r) r^8 \, P(r, \theta) dr \tag{22}$$

On the other hand, the quantity $G(\Gamma) \, d\Gamma$ represents the fraction of the total integrated intensity scattered by all the particles having decay rates from Γ to $\Gamma + d\Gamma$. Hence, we have

$$\int_0^\infty G(\Gamma) d\Gamma = K'\nu \int_0^\infty f^*(r) r^8 P(r, \theta) dr \tag{23}$$

In the histogram method, we devided the Γ-space into segments of an equal interval $\Delta \Gamma$. Thus, the j-th step of the histogram extends from $\Gamma_{j1}(= \Gamma_j - \Delta\Gamma/2)$ to $\Gamma_{j2}(= \Gamma_j + \Delta\Gamma/2)$. To define the corresponding step in r-space, we recall the following two relationships:[9]

$$D(c,r) = \Gamma(c, r)/q^2 = D_0(r)(1 - 0.16 \, c/\rho) \tag{24}$$

$$D_0 = k_B T/6\pi\eta_0 r \tag{25}$$

where D_0 and D are the translational diffusion coefficients at infinite dilution and at total weight concentration c, ρ the particle density, k_B the Boltzmann constant, and η_0 the solvent viscosity. Thus, Γ_{j1} and Γ_{j2} are converted, respectively, to r_{j1} and r_{j2} by using the relationship that

$$r = (k_B T/6\pi\eta_0)(q^2/\Gamma)(1 - 0.16c/\rho) \tag{26}$$

Then, the j-th step in r-space may be defined as

$$r_j = (r_{j1} + r_{j2})/2, \quad \Delta r_j = r_{j1} - r_{j2} \tag{27}$$

and Eq. (23) may be rewritten in the difference form as

$$H_j(\Gamma_j)\Delta\Gamma = K'\nu f^*(r_j) r_j^8 P(r_j, \theta)\Delta r_j \tag{28}$$

We note that the step interval Δr_j is not equal but depends on j. The particle scattering factor $P(r_j, \theta)$ for a rigid sphere is written as

$$P(x) = (3/x^3)^2(\sin x - x \cos x)^2 \tag{29}$$

with

$$x = qr = (4\pi/\lambda)r \sin(\theta/2) \tag{30}$$

where λ is the wavelength in the particle. Eqs. (28) to (30) enables us to determine the unnormalized distribution for the j-th class particles, $f^*(r_j)$, from the histogram $H_j(\Gamma_j)$. The normalized distribution $f(r_j)$ is then calculated as

$$f(r_j) = f^*(r_j) \Big/ \sum_{j=1}^{M} f^*(r_j)\Delta r_j \tag{31}$$

When the distribution consists of two modes, the histogram analysis of $A(\tau)$ is performed by using Eq. (11). The relative intensity of each mode, $a_l(l = 1, 2)$, is then written as

$$a_l = \sum_{j_l=1}^{M_l} H_{jl}(\Gamma_{jl})\Delta\Gamma_l = \sum_{j_l=1}^{M_l} f(r_{jl}) r_{jl}^8 P(r_{jl}, \theta)\Delta r_{jl} \tag{32}$$

with

$$f(r_{jl}) = f^*(r_{jl}) \bigg/ \sum_{l=1}^{2} \sum_{jl=1}^{M_I} f^*(r_{jl}) \Delta r_{jl} \qquad (33)$$

The mean radius $\bar{r}$ and the standard deviation $\mu_{2r}^{1/2}$ of the particle-size distribution either of the total sample or of its constituents may be calculated from $f(r_j)$ or $f(r_{jl})$ by using the ordinary procedure.

2. Experimentals

The detail of our computer-controlled dynamic light scattering instrument with a time interval digitizer has been described earlier.[6] The polymer samples we used were two aqueous suspensions of PS-latex particles of 0.176 and 0.091 μm nominal diameter (Dow Chemical, Lot No. 2M4K and 7EG5, respectively). The dilute suspensions of each particle size were prepared as described earlier.[6] Solutions of desired mixing ratio of 0.091 to 0.176 μm particles were prepared by mixing by weight the constituent suspensions in a light-scattering cell through a Millipore filter of nominal pore size 0.22 μm. Measurements of the autocorrelation function by time interval method were made at $T=25°$ C, $\lambda_0=488$ nm, $\theta=30°$ and $60°$ for the V_v component of scattered light from two mixed suspensions: mixture A; 2.32×10^{-6} g/(g solution) of 0.091 μm particles plus 8.90×10^{-8} g/(g solution) of 0.176 μm particles (weight fraction of 0.091 μm=0.965) and mixture B; 2.45×10^{-6} g/(g soltuion) of 0.091 μm particles plus 4.21×10^{-6} g/(g solution) of 0.176 μm particles (weight fraction of 0.091 μm=0.368). Two single particle suspensions: 1.04×10^{-5} g/(g solution) of 0.091 μm particles and 5.50×10^{-6} g/(g solution) of 0.176 μm particles were also measured for reference to the mixed suspensions.

3. Analysis of Correlation Functions

Results of the histogram analysis for two single aqueous PS-latices are listed in Table III. We used the number of histogram $M=14\sim20$. The reduced decay rates $\bar{\Gamma}/\sin^2(\theta/2)$ obtained at two scattering angles $30°$ and $60°$ were in good agreement within

Table III. Characterization of aqueous suspensions of polystyrene-latex
particles by the histogram method. $T=25°C$; $\lambda_0=488$ nm[a].

angle, degree	$\bar{\Gamma}$, sec^{-1}	$\bar{\Gamma}/\sin^2(\theta/2)$, sec^{-1}	$\mu_2/\bar{\Gamma}^2$, 10^{-3}	$\bar{r}$, 10^{-6} cm	$(\mu_{2r})^{1/2}$,[b] 10^{-6} cm	$\bar{\Gamma}\tau_{max}$
(1) $d=0.176$ μm; $c=5.50 \times 10^{-6}$ g/g solution.						
30	220 ± 3	3290 ± 40	1.49 ± 0.04	8.70 ± 0.10	0.33 ± 0.01	1.67
60	814 ± 2	3260 ± 8	1.73 ± 0.05	8.80 ± 0.01	0.36 ± 0.01	1.67
ref.	—	3278[c]	—	8.80[d]	0.12[d]	—
(2) $d=0.091$ μm; $c=1.04 \times 10^{-5}$ g/g solution.						
30	428 ± 5	6400 ± 70	3.85 ± 0.56	4.47 ± 0.05	0.27 ± 0.02	1.10
60	1610 ± 20	6450 ± 70	6.46 ± 2.44	4.40 ± 0.09	0.36 ± 0.07	1.26
ref.	—	6340[c]	—	4.55[d]	0.29[d]	—

a. Uncertaities represent the standard deviations of the data fitting.

b. $(\mu_{2r})^{1/2}=$(standard deviation of r around $\bar{r}$)$=[\int(r-\bar{r})^2 f^*(r)dr/\int f^*(r)dr]^{1/2}$.

c. Calculated from $\bar{\Gamma}_{calc}=q^2 k_B T/6\pi\eta_0\bar{r}_n$ with $\bar{r}_n$ the nominal radius of Dow Chemical.

d. Nominal values of Dow Chemical.

1.5% with the theoretical values calculated from Eqs. (24) and (25) with $c=0$. The average radii of the particles $\bar{r}$ estimated from $f^*(r)$ by using Eq. (28) agree also within 2~3% with the nominal values of Dow Chemical. Thus, taking the fitting uncertainties indicated in Table III into consideration, we may conclude that, irrespective of the scattering angles, $\bar{\Gamma}$ and $\bar{r}$ obtained are in perfect agreement with Dow Chemical's values determined by electron microscopy. The small values of $\mu_2/\bar{\Gamma}^2$, actually of a order of 10^{-3}, indicate that that the PS-latices used have very narrow size distributions. This is confirmed by comparing the estimated standard deviations $(\mu_{2r})^{1/2}$ with nominal ones as shown in Table III. The tendency that PS-latex particles with a large size give $(\mu_{2r})^{1/2}$ two or three times larger than the nominal value has already been recognized in the histogram analysis by Chu et al.[4]

In Fig. 4 are plotted against Γ the decay rate distribution $H(\Gamma)$ for aqueous PS-latices of $d=0.176$ and 0.091 μm, respectively, at 30° and 60°. The normalized distribution functions of particle size, $f(r)$, are also shown in Fig. 4. It is notable that $f(r)$ derived from $H(\Gamma)$ for two scattering angles have a similar shape of $f(r)$ as it should be.

Results of the histogram analysis for aqueous suspensions of PS-latex mixtures are summarized in Table IV. We used bimodal type of hystograms with $M_1+M_2=7+8$ or $9+12$, where subscripts 1 and 2 denote the particles of $d=0.176$ μm and 0.091 μm, respectively. The average radii $\bar{r}_l$ and standard deviations $(\mu_{2r})_l^{1/2}$ for each mode ($l=1$ and 2) are tabulated in the table. The relative intensities a_1 of the first component with $d=0.176$ μm were also estimated by using Eq. (32). These are to be compared with the calculated intensities $a_{1,calc}=c_1\bar{r}_{1n}^3 P_1(\theta)/[c_1\bar{r}_{in}^3 P_1(\theta)+c_2\bar{r}_{2n}^3 P_2(\theta)]$ where the
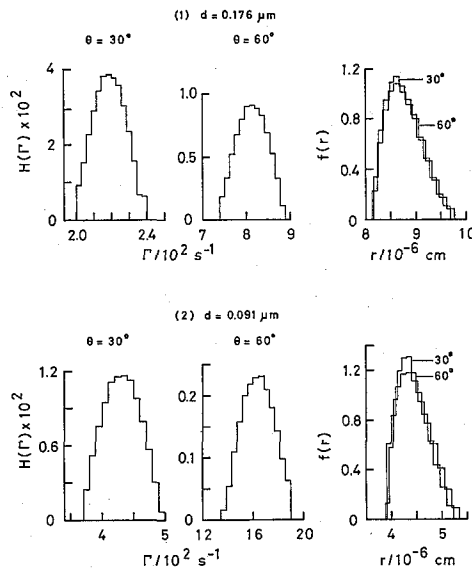

Fig. 4. The histogram $G(\Gamma)$ plotted against the decay rate Γ, and the normalized particle-size distribution $f(r)$ plotted against the particle radius r for the aqueous suspensions of PS-latex particles. (1) The nominal diameter $d=0.176$ μm and (2) $d=0.091$ μm. $T=25°$C, $\lambda_0=488$ nm, and the scattering angle $\theta=30°$ and 60°.

Y. Tsunashima, N. Nemoto, Y. Makita, and M. Kurata

Table IV. Characterization of binary mixtures of aqueous polystyrene-latex particles with different sizes by the histogram method. $T=25°C$; $\lambda_0=488$ nm.[a]

angle,	slow decay mode		fast decay mode		total[b]	
	$\dfrac{\bar{\Gamma}_1}{\sin^2(\theta/2)}$	$(\mu_2/\bar{\Gamma}^2)_1$	$\dfrac{\bar{\Gamma}_2}{\sin^2(\theta/2)}$	$(\mu_2/\bar{\Gamma}^2)_2$	$\dfrac{\bar{\Gamma}}{\sin^2(\theta/2)}$	$\mu_2/\bar{\Gamma}^2$
degree	$\times$ sec	$\times10^3$	$\times$ sec	$\times10^3$	$\times$ sec	$\times10^2$
(1) Mixture A						
$c_2/(c_1+c_2)=0.965$; $c_1=8.90\times10^{-8}$ g/g solution; $c_2=2.32\times10^{-6}$ g/g solution.						
30	3320±40	6.71±0.70	6350±20	4.23±0.39	5740±30	4.90±0.33
60	3250±80	5.57±1.00	6390±40	4.69±1.65	5960±30	3.97±0.56
ref.	3278[c]	—	6340[c]	—	—	—
(2) Mixture B						
$c_2/(c_1+c_2)=0.368$; $c_1=4.21\times10^{-6}$ g/g solution; $c_2=2.45\times10^{-6}$ g/g solution.						
30	3320±30	9.23±1.25	6310±20	2.83±0.79	3540±70	5.32±0.99
60	3260±60	8.73±1.00	6250±60	3.25±1.27	3670±50	7.99±1.55
ref.	3278[c]	—	6340[c]	—	—	—

angle,		slow decay mode		fast decay mode		
	a_1	$\bar{r}_1$	$(\mu_{2r})_1^{1/2}$	$\bar{r}_2$	$(\mu_{2r})_2^{1/2}$	$\bar{\Gamma}\tau_{max}$[b]
degree	$\times10^2$	$\times10^6$ cm	$\times10^6$ cm	$\times10^6$ cm	$\times10^6$ cm	
(1) Mixture A						
30	20.3±1.9	8.57±0.10	0.62±0.05	4.50±0.02	0.29±0.01	1.97
60	13.5±4.1	8.80±0.30	0.64±0.08	4.45±0.04	0.27±0.04	3.12
ref.	20.2(30°)[d] 16.4(60°)[d]	8.80[e]	0.12[e]	4.55[e]	0.29[e]	—
(2) Mixture B						
30	91.4±5.4	8.50±0.09	0.71±0.07	4.56±0.02	0.24±0.03	1.81
60	86.5±4.3	8.71±0.13	0.68±0.08	4.58±0.04	0.26±0.07	1.87
ref.	91.9(30°)[d] 89.7(60°)[d]	8.80[e]	0.12[e]	4.55[e]	0.29[e]	—

a. Uncertainties represent the standard deviations of the data fitting. Subscripts 1 and 2 (except μ_2 and μ_{2r}) denote the particles of $d=0.176\,\mu$m and $0.091\,\mu$m, respectively.

b. Total values obtained when the resulted bimodal distribution is treated as a unimodal one.

c. Calculated from $\bar{\Gamma}_{l,calc}=(k_BT/6\pi\eta_0\bar{r}_{1n})q^2$ with $\bar{r}_{1n}$ the nominal radius of Dow Chemical of l-mode (l=1,2).

d. Calculated from $a_{1,calc}=c_1\bar{r}_{1n}^3P_1(\theta)/[c_1\bar{r}_{1n}^3P_1(\theta)+c_2\bar{r}_{2n}^3P_2(\theta)]$.

e. Nominal values of Dow Chemical.

second subscript n denotes the nominal values. c_1 and c_2 are the concentrations in g/(g solution) of particles with $d=0.176$ and $0.091\,\mu$m, respectively. $\bar{r}_{1n}$ and $\bar{r}_{2n}$ are the nominal radii of Dow Chemical; i.e., $\bar{r}_{1n}=0.088\,\mu$m and $\bar{r}_{2n}=0.0455\,\mu$m, respectively. It is clearly seen from Table IV that $\bar{\Gamma}_l/\sin^2(\theta/2)$ and $\bar{r}_l$ for each mode are, irrespective of scattering angles and of mixed ratio of single suspensions, in good agreement with the corresponding reference values within an error of 2% and 3~4%, respectively. If we take the fitting uncertainties into consideration, we can say that the constitutive $(\mu_{2r})_l^{1/2}$ as well as $\bar{\Gamma}_l$ and $\bar{r}_l$ (l=1,2) at given scattering angles can be fairly well estimated by the histogram method, though $(\mu_{2r})_1^{1/2}$ for larger particles are again overestimated
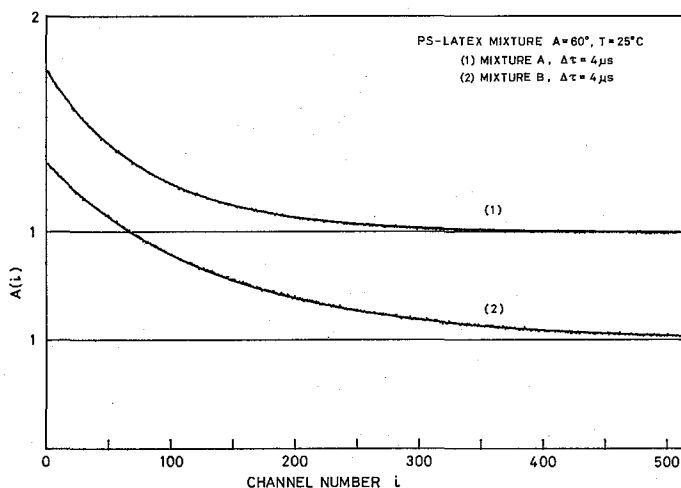
Fig. 5. Plots of $A(i)$ as a function of channel number i obtained for binary mixtures of aqueous PS-latices with different diameters, $d=0.176$ and 0.091 μm, at $T=25°C$, $\lambda_0=488$ nm, and $\theta=60°$: (1) mixture A, fraction of 0.091 μm particles 0.965, $\Delta\tau=4\,\mu$sec; (2) mixture B, fraction 0.368, $\Delta\tau=4\,\mu$sec. The dots denote $A(i)$ and the solid curves represent the fitting curves obtained by the histogram analysis. For the curve (2), its ordinate is sifted downward by 0.5 in order to avoid its overlapping with the curve (1).
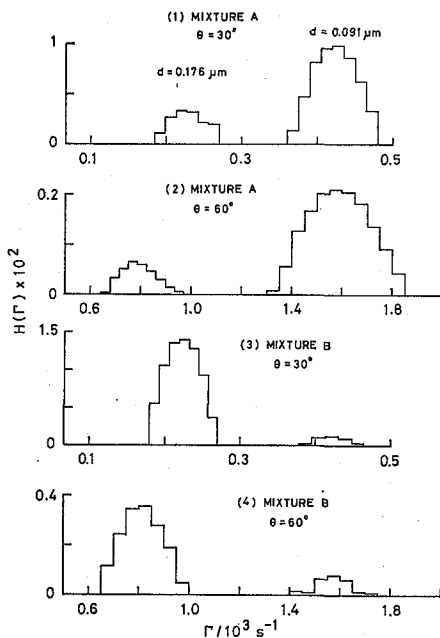
Fig. 6. The histogram $H(\Gamma)$ plotted against the decay rate Γ for binary mixtures of aqueous PS-latices with different diameters, $d=0.176$ and $0.091\,\mu$m: (1) Mixture A; the fraction of $0.091\,\mu$m particles 0.965, $\theta=30°$; (2) mixture A, $\theta=60°$; (3) mixture B, fraction 0.368, $\theta=30°$; (4) mixture B, $\theta=60°$. $T=25°C$ and $\lambda_0=488$ nm.

by a factor of 5 or 6. In addition, it should be emphasized that the relative intensities of each mode evaluated by the histogram method are in good agreement with the theoretically calculated ones to within 5% deviation. Figure 5 shows, as an example, a plot of the measured points of correlation functions $A(i)$ and the fitting curves resulted from the histogram analysis as functions of channel number of clock pulse interval i, which were obtained for two mixed suspensions A and B at $T=25°C$, $\lambda_0=488$ nm and $\theta=60°$.

In Fig. 6, we show plots of $H(\Gamma)$ distribution for two mixed suspensions A and B at scattering angles 30° and 60°, respectively. For each mixture, it can be recognized that the relative histogram area of slow decay mode 1 decreases slightly with increasing scattering angle from 30° to 60° (see, also a_1 in Table IV). This effect may be attributed to more rapid decrease of $P(\theta)$ for 0.176 μm-particles as compared with that for 0.091 μm-particles.

By using Eqs. (32) and (33), we can obtain the normalized size distribution $f(r)$ for mixed suspensions A and B. Figure 7 shows the results, where a pair of $f(r)$ obtained at scattering angles 30° and 60° are plotted against the particle radius r for mixtures A and B. It should be noted in Fig. 7 that the main regions of r for each mode can be definitely settled, irrespective of the scattering angles and of the mixing ratio of two components. That is, the main region for each constituent particles of the present mixtures extends over $r=4\sim5\times10^{-6}$ cm and $r=7.5\sim10\times10^{-6}$ cm for the particles with nominal sizes, $d=0.091$ and 0.176 μm, respectively. This certifies clearly the following situations; (1) the experimental result that $(\mu_{2r})_1^{1/2}$ for mixed suspensions gave 2 times larger deviation than that for single size suspensions (see Tables III and IV) does not exert any substantial change on the shape of $f(r)$ distributions and (2) the individual $f(r)$ estimated from mixed suspensions represents the true size distributions with reasonable accuracy.
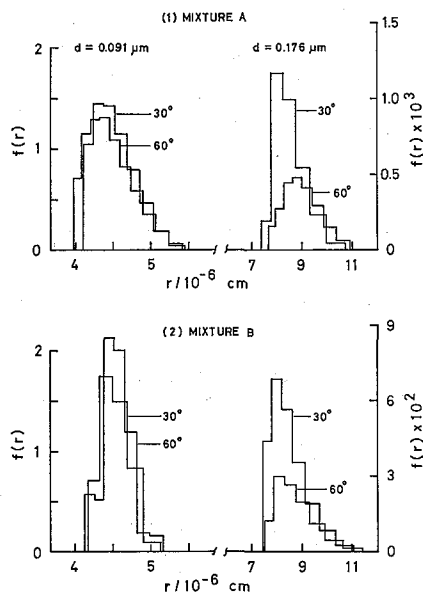

Fig. 7. The normalized particle-size distribution $f(r)$ plotted against particle radius r for binary mixtures of aqueous PS-latices with different diameters: (1) Mixture A, fraction, 0.965; (2) mixture B, 0.368. $T=25°C$, $\lambda_0=488$ nm, and $\theta=30°$ and 60°.

In conclusion, we were able to establish the reliability of the histogram method for the analysis of bimodal distributions of which constituent distributions are both as narrow as $\mu_{2i}/\bar{\Gamma}_i{}^2 = 0.001$ and to show that the relative intensity of each constituent is also determinable from $A(\tau)$ with reasonable accuracy.

ACKNOWLEDGMENTS

REFERENCES AND NOTE

(1) B. J. Berne and R. Pecora, "Dynamic Light Scattering", John Wiley and Sons, Inc., New York, N. Y., 1976.

(2) B. Chu, "Laser Light Scattering", Academic Press, New York, N. Y., 1974.

(3) "Photon Correlation Spectroscopy and Velocimetry", H. Z. Cummins and E. R. Pike, Ed., Plenum Press, New York, N. Y., 1976.

(4) E. Gulari, E. Gulari, Y. Tsunashima, and B. Chu, *J. Chem. Phys.,* **70**, 3965 (1979).

(5) E. Gulari, E. Gulari, Y. Tsunashima, and B. Chu, *Polymer,* **20**, 347 (1979). .

(6) N. Nemoto, Y. Tsunashima, and M. Kurata, *Polymer J.,* **13**, 827 (1981).   This account was presented at the 28th Polymer Symposium of Japan, Tokyo University, May and Osaka University, November 1979.

(7) D. W. Marquardt, *J. Soc. Indust. Appl. Math.,* **11**, 431 (1963).

(8) D. E. Koppel, *J. Chem. Phys.,* **57**, 4814 (1972).

(9) H. Yamakawa, "Modern Theory of Polymer Solutions", Harper and Row, Publishers, New York, N. Y., 1971.

(10) Eq. (28) is reduced from Eq. (21), where the second virial coefficient term of order in c^2 is omitted. This assumption may be acceptable in very dilute solutions such as $c = 10^{-5} \sim 10^{-7}$ g/(g solution) in our experiments.